crystals

MDPI

Article

Elastic, Mechanical and Phonon Behavior of Wurtzite Cadmium Sulfide under Pressure

Melek Güler * and Emre Güler

Department of Physics, Hitit University, Corum 19030, Turkey; eguler71@gmail.com
* Correspondence: mlkgnr@gmail.com; Tel.: +90-3642277000; Fax: +90-3642277005

Academic Editor: Matthias Weil
Received: 27 March 2017; Accepted: 1 June 2017; Published: 4 June 2017

Abstract: Cadmium sulfide is one of the cutting-edge materials of current optoelectronic technology. Although many theoretical works are presented the for pressure-dependent elastic and related properties of the zinc blende crystal structure of cadmium sulfide, there is still some scarcity for the elastic, mechanical, and phonon behavior of the wurtzitic phase of this important material under pressure. In contrast to former theoretical works and methods used in literature, we report for the first time the application of a recent shell model-based interatomic potential via geometry optimization computations. Elastic constants, elastic wave velocities, bulk, Young, and shear moduli, as well as the phonon behavior of wurtzite cadmium sulfide (w-CdS) were investigated from ground state to pressures up to 5 GPa. Calculated results of these elastic parameters for the ground state of w-CdS are approximately the same as in earlier experiments and better than published theoretical data. Our results for w-CdS under pressure are also reasonable with previous calculations, and similar pressure trends were found for the mentioned quantities of w-CdS.

Keywords: CdS; elastic; mechanical; phonon dispersion; wurtzite

1. Introduction

Recently, the computational predictions for materials has become a valuable and rapid way to resolve the unclear subjects of solid state physics. As well, calculating reasonable elastic and thermodynamic results for materials can substitute the impossible and expensive experiments and may provide deeper insights for the concerned materials [1–5].

The focus of the present work is a CdS compound from the II-VI semiconductor family (i.e., CdS, CdSe, and CdTe) which has widespread technological applications ranging from solar cells to light emitting diodes [6]. Further, under ambient conditions, CdS can crystallize in either zinc blende (ZB) crystal structure with space group F-43m or wurtzite (w) crystal structure with $P6_3mc$ space group [7–11]. Moreover, as reported in recent experimental measurements [12], phase transition from the ZB phase to the wurtzite phase of CdS occurs between the pressure values 3.0 GPa and 4.3 GPa.

It is possible to find a number of works performed especially for the mechanical, elastic, thermodynamic, and other properties of ZB CdS compounds not only with experiments, but also with theoretical works due to its simple crystal structure [6]. In 2000, Benkabou et al. [7] surveyed the structural and elastic properties of several II-VI compounds (CdS, CdSe, ZnS, and ZnSe) in ZB phase with their determined Tersoff potential parameters. Later, in 2004, Wright and Gale [11] introduced their interatomic potentials for the structural and stability properties of ZB and w-CdS under zero Kelvin temperature and zero pressure (ground state conditions). Afterwards, in 2006, Deligoz et al. [8] performed norm-conserving pseudopotential density functional theory (DFT) calculations for ZB phase of CdX (X: S, Se, Te) compounds in their ground states. In 2011, Ouendadji and coworkers [6] computed the structural, electronic, and thermal characteristics of the ZB phase of CdS, CdSe, and CdTe

compounds in their DFT studies by using full potential linearized augmented plane wave (FP-LAPW) through local density approximation (LDA) and the generalized gradient approximation (GGA) in their ground state. Grünwald et al. [9] also established transferable pair potentials for CdS and ZnS crystals to accurately describe the ground state features of ZB and w-CdS compounds in 2012. At the same time, Tan et al. [10] documented the effect of pressure and temperature on ZB and w-CdS structures in their plane-wave pseudopotential DFT study with LDA, including phase transition pressure, entropy, enthalpy, elasticity, free energy, and heat capacity. As is clear from these works, former investigations strictly focus on the ground state properties of the ZB CdS compound where w-CdS and its important physical properties under pressure are still lacking.

In this research, we therefore concentrate on the elastic, mechanical, and phonon properties of w-CdS under pressure. Contrary to the above applied methods and employed potentials of literature, we report for the first time the use of a recent shell model-type interatomic potential [13] to determine the mentioned high-pressure quantities of w-CdS with geometry optimization calculations. During our work, we considered the elastic constants, bulk modulus, shear modulus, and Young modulus, elastic wave velocities, mechanical stability conditions, and phonon properties of w-CdS under pressures between 0 GPa and 5 GPa at T = 0 K.

The next part of the manuscript (Section 2) gives a short outline for the geometry optimization and other details of present computations. Subsequently, Section 3 affords our results and earlier data on the calculated quantities of w-CdS with discussion. At the end, Section 4 summarizes the key results of the present survey in the conclusion of the paper.

2. Computational Methods

For crystals, geometry optimization is an effective and practical method utilized in both molecular dynamics (MD) and DFT computations to obtain a stable arrangement of periodic systems or molecules with rapid energy computations. The basic concept for geometry optimization deals with the repeated potential energy sampling in which energy shows a minimum and all acting forces on total atoms reach zero. Detailed information for geometry optimization method and further points can also be obtained from References [14–17].

All of the computations of this work were performed with the General Utility Lattice Program (GULP) 4.2 MD code. GULP can be used for wide-range property computations of periodic solids, surfaces, and clusters by applying an appropriate interatomic potential relevant to the demands of the research [14–17].

The most accurate and reliable results of computer simulations are strongly linked with the quality of the employed interatomic potentials during computations [18]. Besides, shell model-form interatomic potentials provide reasonable outcomes on both ground state and high-pressure features of fluorides, oxides, and other compounds [19,20]. Since the shell model and its methodologies are well-known [14–20], we present only a short explanation here. Most of the shell model potentials involve long-range Coulomb and short-range pairwise interactions, and their ionic polarization is treated by Dick and Overhauser [21]. Further, in the shell model, an atom is characterized by two discrete components: the core (signifies the core and nucleus electrons) and the shell (stands for the valence electrons). The core and the shell independently interact with other atoms and with each other. Therefore, the interaction potential used in this work was in the form of:

$$U_{ij} = \frac{q_i q_j}{r_{ij}} + A \exp\left(-\frac{r_{ij}}{\rho}\right) - \frac{C}{r_{ij}^6}$$

where the first term in the equation denotes the Coulomb interaction, the second term symbolizes the repulsive interaction of the overlapping electron clouds, and the third term holds for the van der Waals interaction. Additionally, A, ρ, and C are the particular Buckingham potential interaction parameters,

where Coulomb interactions follow the Ewald summation method [22]. For more information and other conjectures, interested readers can see References [23–26].

A recent shell model-type interatomic potential [13] was employed in this work, which is originally derived from DFT calculations for the bulk properties of CdS, CdSe, PbS, and PbSe solid compounds as well as their mixed phases. To keep the original form of the applied potential, we also ignored the shell-shell interactions during the present research, as in Reference [13]. Further, Table 1 lists the present potential parameters employed in our calculations, and further details about the parameterization procedure of this potential can be also found in Reference [13]. The cell parameters of w-CdS were assigned as a = 4.13 Å and c = 6.63 Å, as seen in Figure 1 which is visualized with VESTA 3.0 [27]. Constant pressure optimization was applied to our work to avoid constraints for an efficient geometry optimization [14–17]. Additionally, cell geometries were optimized by Newton–Raphson procedure generated from the Hessian matrix. The Hessian matrix obtained from second derivatives of the energy was iteratively updated with the default BFGS algorithm [28–31] of GULP. After fixing the prerequisites for w-CdS crystal structure and initial optimization settings, we have performed various runs by ensuring the pressure values change from 0 GPa to 5 GPa with 0.5 GPa steps at zero Kelvin temperature.

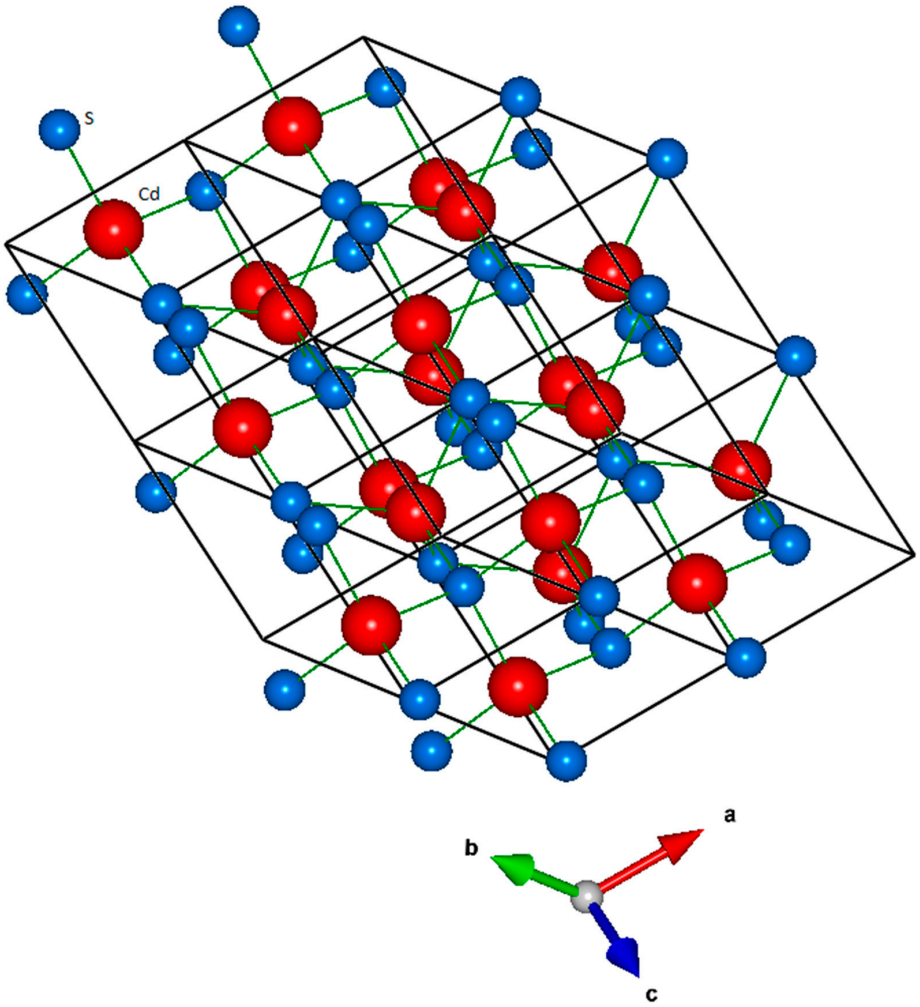

Figure 1. Crystal structure of wurtzitic CdS (w-CdS). Blue atoms show sulphur anions where red atoms represent cadmium cations along a, b, and c axes.

During our work, phonon and connected features of w-CdS were also considered after geometry optimizations as a function of external pressure through quasiharmonic approximation under zero temperature, as implemented in GULP. It is feasible to calculate the phonon density of states (PDOS) as

well as phonon dispersions for a given material following the statement of a shrinkage factor via GULP phonon calculations. Besides, GULP defines the phonons by computing their values at special points in reciprocal space in the first Brillouin zone. To attain the Brillouin zone integration and determine the PDOS, we have employed a Monkhorts and Pack scheme [32] routine with $8 \times 8 \times 8$ *k-point* mesh.

Table 1. Shell model-type interatomic potential parameters taken from Reference [13]. The short-range interactions between shells (s) are ignored. The effective core (c) charges are assigned as 0.8e for Cd and −0.8e for S. A potential cut-off with radius 12 Å was set for short-range interactions.

Interaction	A (eV)	ρ (Å)	C (eV·Å^6)
Cd_C-S_C	1.26×10^9	0.107	53.5
S_C-S_C	4.68×10^3	0.374	120

3. Results and Discussion

Figure 2 represents the density behavior of w-CdS under pressure. The density of many materials displays straight increments under pressure due to the volume reduction of the related crystal. This fact is also valid for w-CdS under pressure, as seen in Figure 2. The lowest density value of w-CdS is 4.89 g/cm^3 for 0 GPa, and the highest density value at 5 GPa is 5.2 g/cm^3 at zero temperature. The presently obtained ground state (T = 0 K and P = 0 GPa) value of density with 4.89 g/cm^3 of w-CdS is comparable to the room temperature experimental density value of 4.82 g/cm^3 [33].

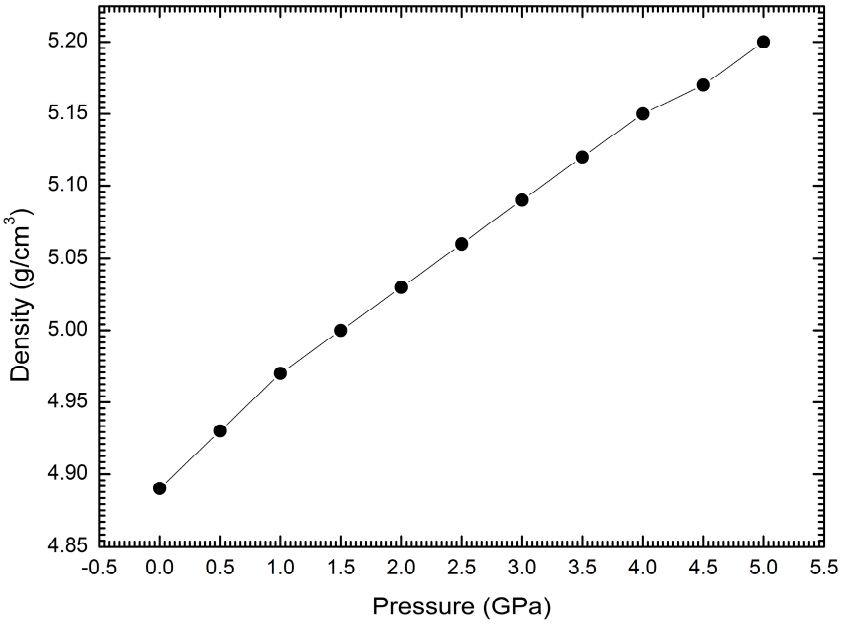

Figure 2. Density behavior of w-CdS under pressure.

After optimizing the structure of a given material, it is then possible to compute different physical features with GULP. These calculations comprise the elastic constants, bulk modulus, and other mechanical quantities (shear modulus and Young moduli, elastic wave velocities, etc.) of the regarding material. For instance, the presently calculated elastic constants show the second derivatives of the energy density with respect to strain, and details about other remaining property calculations can be also found within Reference [16].

Elastic constants deliver clear perceptions about the mechanical and other associated properties of materials. Though elastic constants obtained from total energy computations belong to single crystal values, it is crucial to get accurate polycrystalline elastic constants of materials because many technically

important materials exist in polycrystalline form [34]. For this reason, Voigt–Reuss–Hill [35–37] values were considered during this work.

For wurtzite crystals, five well-known elastic constants exist, which are specified as C_{11}, C_{12}, C_{13}, C_{33}, and C_{44} [38].

Figure 3 indicates our findings for C_{11}, C_{12}, C_{13}, C_{33}, and C_{44} constants for w-CdS under pressures between 0 GPa and 5 GPa. Among them C_{11} and C_{33} represent the longitudinal elastic character where elastic wave propagation occurs easily under pressure. This easiness causes the increments of C_{11} and C_{33} under pressure. Surprisingly, the magnitudes of C_{11} and C_{33} are similar to each other in the ground state, and the gap between them becomes greater as the pressure increases. Unlike C_{11} and C_{33}, C_{44} constant (characterizing the shear elastic response to retarded wave propagation) has a sluggish decrement. Figure 3 also shows that the calculated elastic constants are in the range of $C_{33} > C_{11} > C_{12} > C_{13} > C_{44}$. Both the range of the elastic constants and the slight decrement of the C_{44} constant under pressure mimic the DFT findings of Tan et al. [10]. However, our results for the ground state parameters of w-CdS are obviously satisfactory compared to those of by Tan et al. [10] as well as Wright and Gale [11], and much closer to the experimental results of Bolef et al. [39] as listed in Table 2.

According to stability, the proverbial Born mechanical stability criterion for hexagonal crystals is also valid for wurtzite crystals, and must fulfill [38]:

$$C_{44} > 0, C_{11} > |C_{12}| \text{and } (C_{11} + 2\,C_{12})\,C_{33} > 2C_{13}^{2}$$

Presently calculated results of elastic constants of w-CdS obey the mechanical stability criterion (Figure 3 and Table 2), which consequently indicates that the w-CdS is mechanically stable in its ground state.

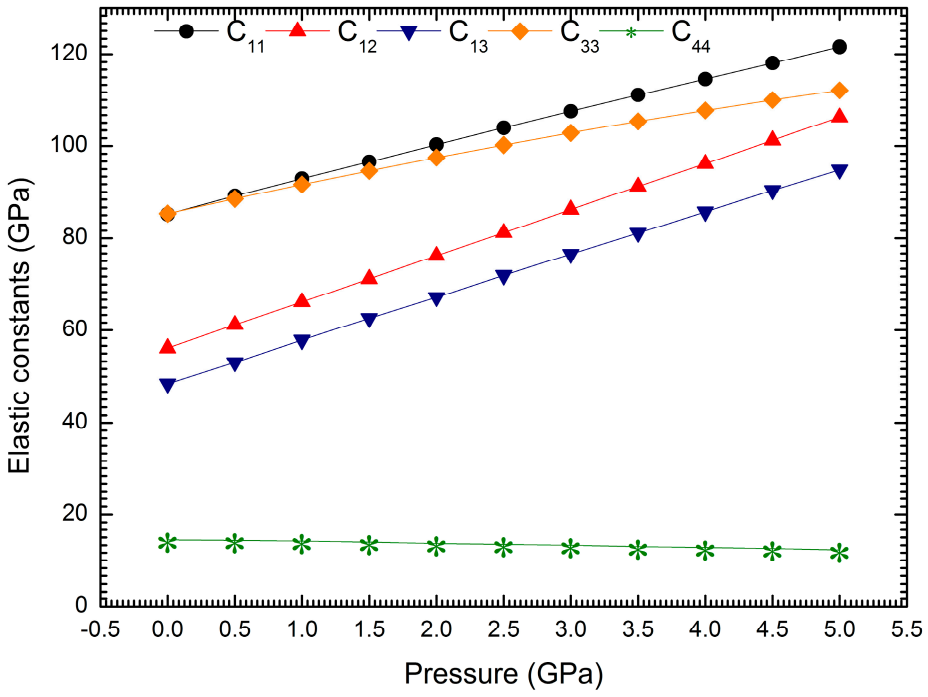

Figure 3. Elastic constants of w-CdS under pressure.

Bulk modulus (B) is an essential elastic constant connected to the bonding strength and is used as a primary parameter for the calculation of a material's hardness. Shear modulus (G) is the measure of the resistivity of a material after applying a shearing force. Furthermore, Young modulus (E) also defines the amount of a material's resistance to uniaxial tensions. These three distinct moduli (B, G,

and *E*) are other valuable parameters for classifying the mechanical properties of materials. Figure 4 shows the bulk modulus, Young modulus, and shear modulus (*B*, *E*, and *G*) of w-CdS under pressure. From the common physical expression of bulk modulus $\left(B = \Delta\frac{P}{\Delta}V\right)$, it is not difficult to predict a raise for *B* due to its direct proportion to pressure. So, the bulk modulus of w-CdS represents a clear increment with pressure. Conversely, *G* and *E* moduli have insignificant decrements under pressure, again similar to the DFT findings of Tan et al. [10]. Moreover, Table 2 also lists numerical comparisons for *B*, *G*, and *E* moduli of current and earlier data of w-CdS under zero temperature and pressure. Our results for *B*, *G*, and *E* moduli agree with both experiments and other DFT results, as seen in Table 2.

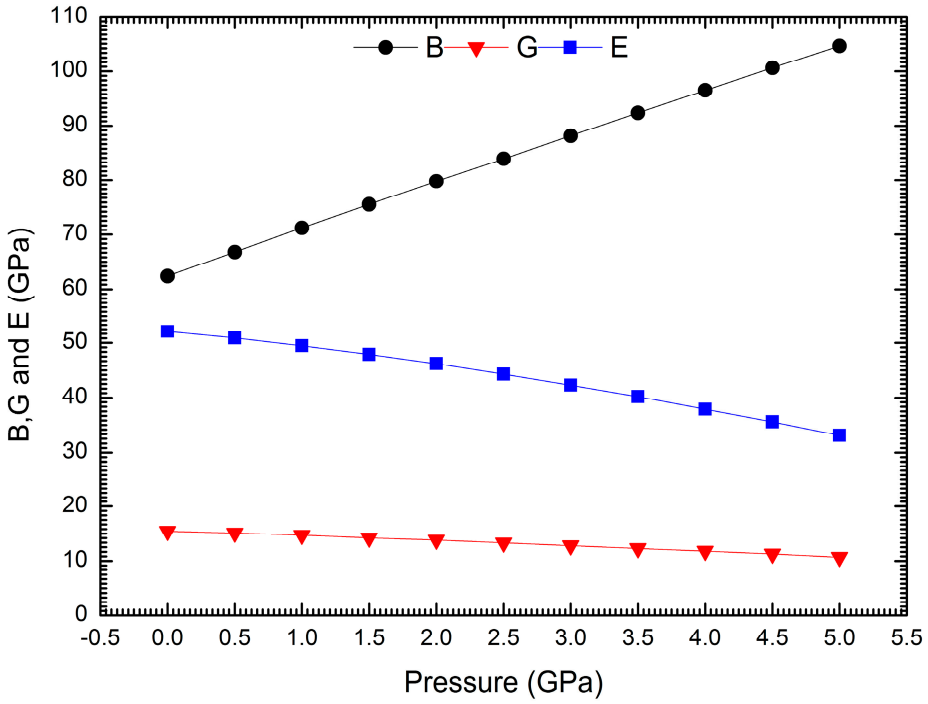

Figure 4. Elastic moduli (*B*, *G*, and *E*) behavior of w-CdS versus pressure.

Ductile and brittle responses of materials represent two antithetical mechanical characteristics of solids when they exposed to external stress. Since these adjectives (ductility and brittleness) are important for the production of desired materials, we also checked the ductile (brittle) behavior of w-CdS under pressure. Usually, brittle materials display a considerable resistance to the deformation before fracture, whereas ductile materials can be easily deformed. In addition, Pugh ratio evaluation [40] is one of the prevalent routines in the literature which conveys a decisive limit for ductile (brittle) performance of materials. As stated by Pugh, a material can be ductile if its G/B ratio is smaller than 0.5; otherwise, it can be brittle. Our careful assessment shows that G/B values decrease from 0.24 (P = 0 GPa) to 0.10 (P = 5 GPa) at zero temperature for w-CdS as in Figure 5. So, w-CdS behaves in a ductile manner for the entire pressure range.

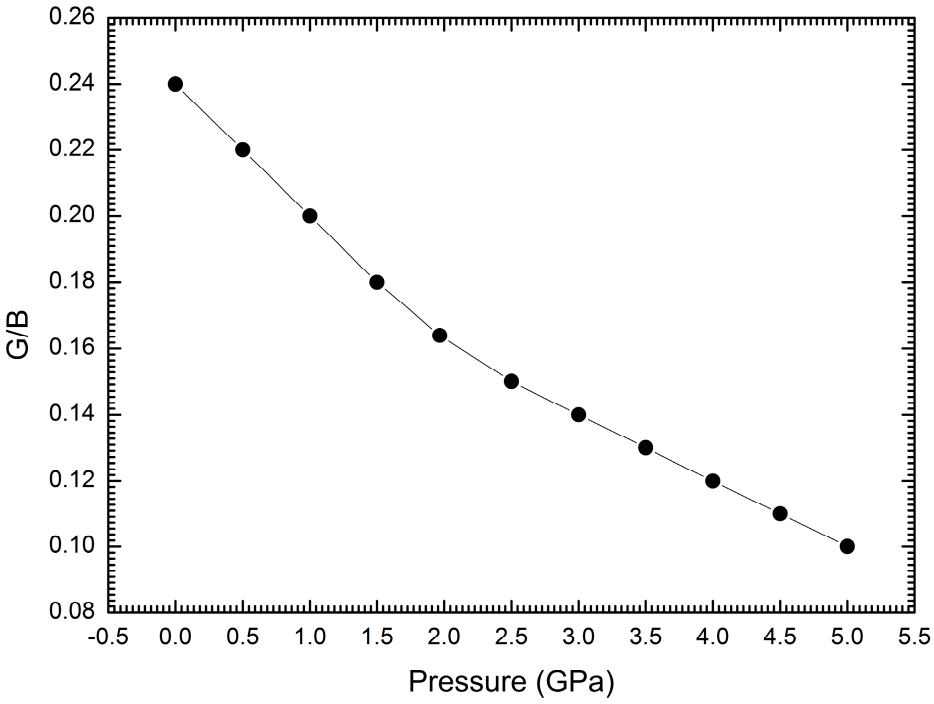

Figure 5. G/B ratio of w-CdS against pressure.

Longitudinal and shear elastic waves may arise in solids at low temperatures due to vibrational excitations originating from the acoustic modes [20]. Thus, V_L signifies the longitudinal elastic wave velocity, where V_S stands for the shear wave velocity. Figure 6 represents the pressure behavior of V_L and V_S of w-CdS pressure at T = 0 K. As is clear in Figure 6, V_L has a significant increment compared to V_S, and this is the most common case for materials because of the facts explained above. Obtained data of this work for both V_L and V_S are again reasonable when compared to previous experiments (See Table 2).

Table 2. Comparing the present results with former experimental and theoretical data for the calculated parameters of w-CdS at zero pressure and temperature.

Parameter	Exp [33]	Present	Ref [9]	Ref [10]	Ref [11]	Ref [41]
C_{11} (GPa)	84.3	85.2	107.3	93.9	102.8	80.5
C_{12} (GPa)	52.1	56.2	35.8	57.6	45.4	45.0
C_{13}(GPa)	46.3	48.4	15.9	50.1	47.5	37.1
C_{33} (GPa)	93.9	85.3	144.3	105.2	113.3	87.0
C_{44} (GPa)	14.8	14.5	20.5	15.8	32.4	15.2
B (GPa)	62.7	62.4	54.0	68.9	66.4	54.0
E (GPa)	48.1	52.0		51.0		
G (GPa)	-	15.4		18.5		
V_S (km/s)	1.84	1.77				
V_L (km/s)	4.24	4.11				

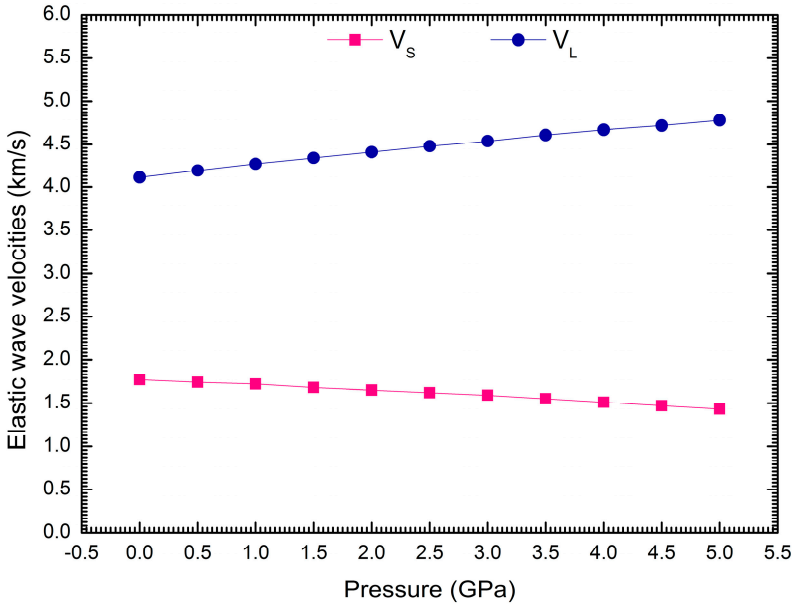

Figure 6. Behavior of longitudinal (V_L) and shear wave (V_S) velocities of w-CdS under pressure.

The success of the present potential on the ground state phonon dispersion properties of w-CdS have already been quantitatively compared in its original reference [13] with experimental results. Additionally, we would like to present the missing ground state phonon density of states (PDOS) of w-CdS to explain the contribution of both elements S and Cd to the phonon properties of the compound. Figure 7 displays the partial and total PDOS of w-CdS in the ground state. In Figure 7, the phonon density of states appear with four well-separated regions corresponding to the longitudinal and transverse acoustic modes (LA and TA) and longitudinal and transverse optic modes (LO and TO) of w-CdS. Besides, the contribution of the Cd element to acoustic phonon modes is higher than S, whereas the opposite case is valid for the S element due to its dominant contribution to optical modes. There is also a clear gap between the frequencies 150 cm^{-1} and 250 cm^{-1} originating from the mass differences of Cd and S elements of w-CdS.

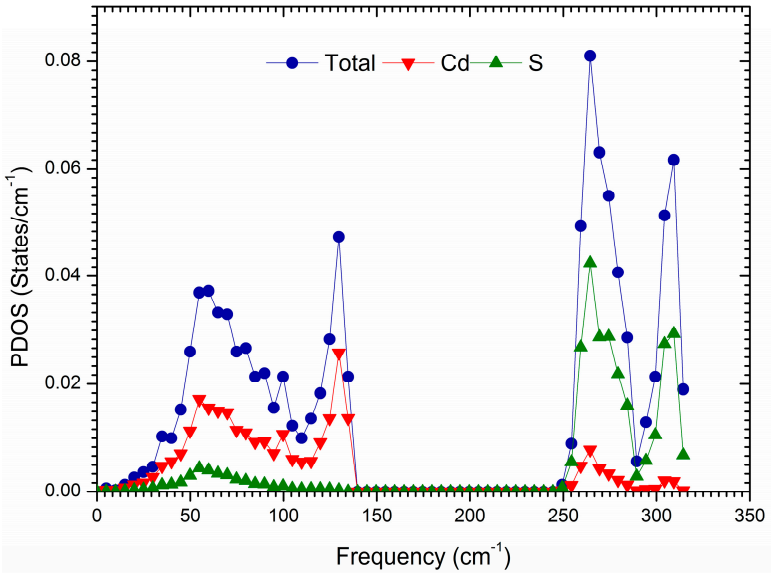

Figure 7. Partial and total phonon density of states of (PDOS) curve of w-CdS under zero temperature and pressure.

On the other hand, Figure 8 shows the phonon dispersion of w-CdS along the chosen Γ-A path (as same as with original Ref [13]) in reciprocal space for pressures 0 GPa, 1 GPa, 3 GPa, and 5 GPa. As is evident in Figure 8, each pressure value above 0 GPa slightly shifts the phonon dispersion curves of w-CdS to higher frequency values of due to atoms which move towards to each other and sit in steeper potential wells under pressure. The corresponding PDOS curves of applied pressures are also given in Figure 9. The increasing pressure also increases the PDOS peaks of w-CdS for each pressure, and under pressure, the gap between acoustic and optical modes shifts to higher frequencies from 150 cm^{-1} to 275 cm^{-1}.

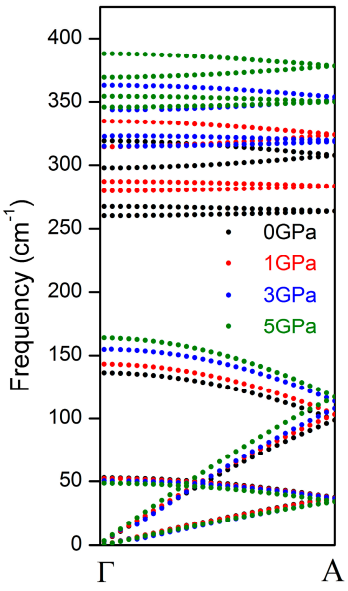

Figure 8. Phonon dispersion curve of w-CdS at zero temperature under pressures 0 GPa, 1 GPa, 3 GPa, and 5 GPa.

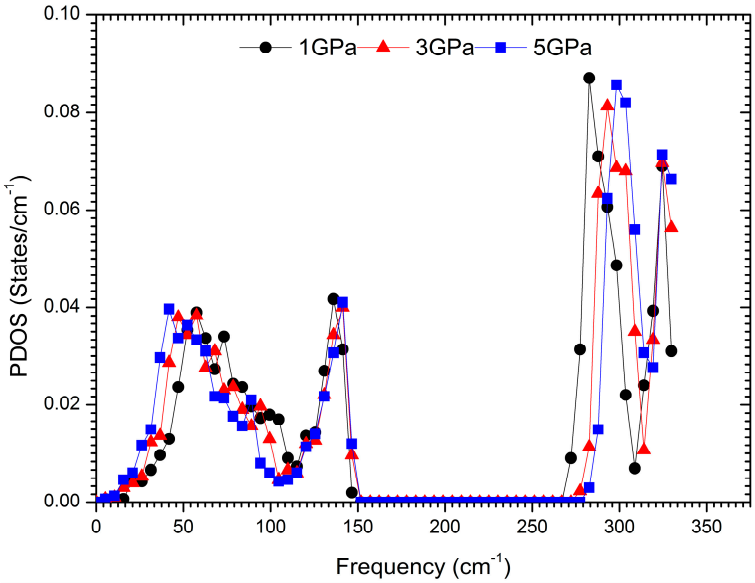

Figure 9. Phonon density of states of (PDOS) curve of w-CdS at zero temperature for 1 GPa, 3 GPa, and 5 GPa.

Overall, our results for this research demonstrate a fair accordance with the experiments—especially for elastic constants, bulk modulus, elastic wave velocities, and phonon

properties of w-CdS in its ground state. Finally, the presented results for all calculated parameters of w-CdS through this work are both consistent with experiments and better than those of some published theoretical data.

4. Conclusions

In summary, we applied a recent shell model-type interatomic potential for the first time with geometry optimization calculations to study both ground state and pressure-dependent elastic, mechanical, and phononic aspects of w-CdS. As the present results prove, the application of this potential which is originally employed for computing the ground state bulk properties of w-CdS also successfully captures the investigated properties under pressure. Particularly, present results for the ground state of w-CdS are about former experiments for the elastic constants, bulk modulus, elastic wave velocities, and phonon characteristics and better than those of other published theoretical data. Moreover, the effect of pressure on w-CdS was also presented and reasonable results were obtained for several properties of w-CdS after benchmarking the existing literature. Bulk modulus, shear modulus, and other longitudinal wave-related elastic and mechanical quantities show clear increments under pressure, where the shear wave connected parameters display sluggish decrements due to the nature of longitudinal and shear elastic waves propagation. w-CdS exhibits ductile character in its ground state and even under pressure. We hope that our results add value to the forthcoming researches about w-CdS under pressure.

Author Contributions: Melek Güler and Emre Güler conceived and designed the theoretical calculations; Melek Güler performed the all calculations; Melek Güler analyzed the all obtained data of work; both Melek Güler and Emre Gülerwrote the paper.

Conflicts of Interest: The authors declare no conflict of interest.

References

1. Ullah, N.; Ullah, H.; Murtaza, G.; Khenata, R.; Ali, S. Structural phase transition and optoelectronic properties of ZnS under pressure. *J. Opt. Adv. Mater.* **2015**, *17*, 1272.
2. Bouhemadou, A.; Haddadi, K.; Khenata, R.; Rached, D.; Bin-Omran, S. Structural, elastic and thermodynamic properties under pressure and temperature effects of MgIn2S4 and CdIn2S4. *Phys. B Condens. Matter* **2012**, *407*, 2295. [CrossRef]
3. Seddik, T.; Semari, F.; Khenata, R.; Bouhemadou, A.; Amrani, B. High pressure phase transition and elastic properties of Lutetium chalcogenides. *Phys. B Condens. Matter* **2010**, *405*, 394. [CrossRef]
4. Duan, D.; Liu, Y.; Ma, Y.; Liu, Z.; Cui, T.; Liu, B.; Zou, G. Ab initio studies of solid bromine under high pressure. *Phys. Rev. B* **2007**, *76*, 104113. [CrossRef]
5. Duan, D.; Huang, X.; Tian, F.; Li, D.; Yu, H.; Liu, Y.; Ma, Y.; Liu, B.; Cui, T. Pressure-induced decomposition of solid hydrogen sulfide. *Phys. Rev. B* **2015**, *91*, 180502(R). [CrossRef]
6. Ouendadji, S.; Ghemid, S.; Meradji, H.; El Haj Hassan, F. Theoretical study of structural, electronic, and thermal properties of CdS, CdSe and CdTe compounds. *Comput. Mater. Sci.* **2011**, *50*, 1460. [CrossRef]
7. Benkabou, F.; Aourag, H.; Certier, M. Atomistic study of zinc-blende CdS, CdSe, ZnS, and ZnSe from molecular dynamics. *Mater. Chem. Phys.* **2000**, *66*, 10–16. [CrossRef]
8. Deligoz, E.; Colakoglu, K.; Ciftci, Y. Elastic, electronic, and lattice dynamical properties of CdS, CdSe, and CdTe. *Phys. B Condens. Matter* **2006**, *373*, 124–130. [CrossRef]
9. Grünwald, M.; Zayak, A.; Neaton, J.B.; Geissler, P.L.; Rabani, E. Transferable pair potentials for CdS and ZnS crystals. *J. Chem. Phys.* **2012**, *136*, 234111. [CrossRef] [PubMed]
10. Tan, J.J.; Li, Y.; Ji, G.F. High-Pressure Phase Transitions and Thermodynamic Behaviors of Cadmium Sulfide. *Acta Phys. Pol. A* **2011**, *120*, 501–506. [CrossRef]
11. Wright, K.; Gale, J.D. Interatomic potentials for the simulation of the zinc-blende and wurtzite forms of ZnS and CdS: Bulk structure, properties, and phase stability. *Phys. Rev. B* **2004**, *70*, 035211. [CrossRef]
12. Li, Y.; Zhang, X.; Li, H.; Li, X.; Lin, C.; Xiao, W.; Liu, J. High pressure-induced phase transitions in CdS up to 1 Mbar. *J. Appl. Phys.* **2013**, *113*, 083509. [CrossRef]

13. Fan, Z.; Koster, R.S.; Wang, S.; Fang, C.; Yalcin, A.O.; Tichelaar, F.D.; Zandbergen, H.W.; van Huis, M.A.; Vlugt, T.J.H. A transferable force field for CdS-CdSe-PbS-PbSe solid systems. *J. Chem. Phys.* **2014**, *141*, 244503. [CrossRef] [PubMed]
14. Gale, J.D. Empirical potential derivation for ionic materials. *Philos. Mag. B* **1996**, *73*, 3–19. [CrossRef]
15. Gale, J.D. GULP: A computer program for the symmetry-adapted simulation of solids. *J. Chem. Soc. Faraday* **1997**, *93*, 629. [CrossRef]
16. Gale, J.D.; Rohl, A.L. The General Utility Lattice Program (GULP). *Mol. Simulat.* **2003**, *29*, 291. [CrossRef]
17. Gale, J.D. GULP: Capabilities and prospects. *Z. Kristallogr.* **2005**, *220*, 552. [CrossRef]
18. Walsh, A.; Sokol, A.A.; Catlow, C.R.A. *Computational Approaches to Energy Materials*, 1st ed.; John Wiley & Sons, Ltd.: West Sussex, UK, 2013; p. 101.
19. Valerio, M.E.G.; Jackson, R.A.; de Lima, J.F. Derivation of potentials for the rare-earth fluorides, and the calculation of lattice and intrinsic defect properties. *J. Phys. Condens. Matter* **2000**, *12*, 7727. [CrossRef]
20. Güler, E.; Güler, M. High pressure elastic properties of wurtzite aluminum nitrate. *Chin. J. Phys.* **2014**, *52*, 1625–1635.
21. Dick, B.G.; Overhauser, A.W. Theory of the Dielectric Constants of Alkali Halide Crystals. *Phys. Rev.* **1958**, *112*, 90. [CrossRef]
22. Ewald, P.P. Die Berechnung optischer und elektrostatischer Gitterpotentiale. *Ann. Phys.* **1921**, *64*, 253. [CrossRef]
23. Archer, T.D.; Birse, S.E.A.; Dove, M.T.; Redfern, S.; Gale, J.D.; Cygan, R.T. An interatomic potential model for carbonates allowing for polarization effects. *Phys. Chem. Miner.* **2003**, *30*, 416. [CrossRef]
24. Ayala, A.P. Atomistic simulations of the pressure-induced phase transitions in BaF2 crystals. *J. Phys. Condens. Matter* **2001**, *13*, 11741. [CrossRef]
25. Chisholm, J.A.; Lewis, D.W.; Bristowe, P.D. Classical simulations of the properties of group-III nitrides. *J. Phys. Condens. Matter* **1999**, *11*, L235–L239. [CrossRef]
26. Kilo, M.; Jackson, R.A.; Borchardt, G. Computer modelling of ion migration in zirconia. *Phil. Mag.* **2003**, *83*, 3309. [CrossRef]
27. Momma, K.; Izumi, F. VESTA 3 for three-dimensional visualization of crystal, volumetric and morphology data. *J. Appl. Crystallogr.* **2011**, *44*, 1272–1276. [CrossRef]
28. Broyden, G.C. The Convergence of a Class of Double-rank Minimization Algorithms 1. General Considerations. *J. Inst. Math. Appl.* **1970**, *6*, 76. [CrossRef]
29. Fletcher, R. A new approach to variable metric algorithms. *Comput. J.* **1970**, *13*, 317. [CrossRef]
30. Goldfarb, D. A family of variable-metric methods derived by variational means. *Math. Comput.* **1970**, *24*, 23. [CrossRef]
31. Shanno, D.F. Conditioning of quasi-Newton methods for function minimization. *Math. Comput.* **1970**, *24*, 647. [CrossRef]
32. Monkhorst, H.J.; Pack, J.D. Special points for Brillouin-zone integrations. *Phys. Rev. B* **1976**, *13*, 5188. [CrossRef]
33. Adachi, S. *Handbook on Physical Properties of Semiconductors*; Kluwer: Boston, MA, USA, 2004; Volume 1.
34. Hirsekorn, S. Elastic properties of polycrystals. *Textures Microstruct.* **1990**, *12*, 1–14. [CrossRef]
35. Voigt, W. *Lehrbuch der Kristallphysik*; B.G. Teubner: Leipzig, Germany, 1928.
36. Reuss, A. Berechnung der Fließgrenze von Mischkristallen auf Grund der Plastizitätsbedingung für Einkristalle. *Angew. Z. Math. Mech.* **1929**, *9*, 55. [CrossRef]
37. Hill, R. The Elastic Behaviour of a Crystalline Aggregate. *Proc. Phys. Soc. A* **1952**, *65*, 349. [CrossRef]
38. Born, M.; Huang, K. *Dynamical Theory of Crystal Lattices*; Clarendon: Oxford, UK, 1956.
39. Bolef, D.I.; Melamed, N.T.; Menes, M. Elastic constants of hexagonal cadmium sulfide. *J. Phys. Chem. Solids* **1960**, *17*, 143. [CrossRef]
40. Pugh, S.F. Relations between the elastic moduli and the plastic properties of polycrystalline pure metals. *Philos. Mag.* **1954**, *45*, 823. [CrossRef]
41. Guo, X.J.; Xu, B.; Liu, Z.Y.; Yu, D.L.; He, J.L.; Guo, L.C. Theoretical Hardness of Wurtzite-Structured Semiconductors. *Chin. Phys. Lett.* **2008**, *25*, 2158.